

The surface brightness profile of the remote cluster NGC 2419 (Research Note)

M. Bellazzini¹

INAF - Osservatorio Astronomico di Bologna, Via Ranzani 1, 40127 Bologna, Italy
e-mail: michele.bellazzini@oabo.inaf.it

Accepted by A&A, July 17, 2007

ABSTRACT

Context. It is well known that the bright and remote Galactic globular cluster NGC 2419 has a very peculiar structure. In particular its half-light radius is significantly larger than that of ordinary globular clusters of similar luminosity, being as large as that of the brightest nuclei of dwarf elliptical galaxies.

Aims. In this context it is particularly worth to check the reliability of the existing surface brightness profiles for this cluster and of the available estimates of its structural parameters.

Methods. Combining different datasets I derive the surface brightness profile going from the cluster center out to $\approx 480''$, i.e. ≈ 25 core radii (r_c). The profile of the innermost $21''$ has been obtained from aperture photometry from four different Hubble Space Telescope ACS/WFC images. Outside of this radius, the profile has been obtained from star counts.

Results. The newly obtained surface brightness profile is in excellent agreement with that provided by Trager, King & Djorgovski for $r \gtrsim 4''$. The new profile is best fitted by a King model having $r_c = 0.32'$ ($\sim 5\%$ smaller than previous estimates), central surface brightness $\mu_V(0) = 19.55$ and concentration $C = 1.35$. Also new independent estimates of the total integrated V magnitude ($V_t = 10.47 \pm 0.07$) and of the half-light radius ($r_h = 0.96' \pm 0.2'$) have been obtained. The average ellipticity in the range $5'' \leq r \leq 120''$ is $\langle \epsilon \rangle = 0.19 \pm 0.14$. If the four points of the ellipticity profile that deviates more than 2σ from the overall mean are excluded, $\langle \epsilon \rangle = 0.14 \pm 0.07$ is obtained.

Conclusions. The structure of NGC2419 is now reliably constrained by (at least) two fully independent observational profiles that are in good agreement one with the other. Also the overall agreement between structural parameters independently obtained by different authors is quite satisfying.

Key words. (Galaxy): globular clusters: individual: NGC 2419

1. Introduction

NGC 2419 is one of the brightest globular clusters (GC) of the Milky Way and it is located at very large distance from the center of the Galaxy ($R_{GC} = 91.5$ kpc, see Harris (1996)). Moreover, it is well known that it has a quite peculiar structure: its half-light radius is much larger (by a factor of ~ 5) than that of other GCs of the same luminosity, being as large as that of the largest nuclei of dwarf elliptical galaxies, or the scale sizes of Ultra Compact Dwarfs (Mackey & van den Bergh (2005), Federici et al. (2007), Evstigneeva et al. (2007) and references therein; see Fig. 13 of van den Bergh (1995) for a direct visual demonstration of the extra-large size of the cluster). For these reasons, it has been proposed that NGC 2419 is in fact the remnant nucleus of a dwarf elliptical satellite of the Milky Way that was partially disrupted by the Galactic tidal field (Mackey & van den Bergh (2005), but see Ripepi et al. (2007) for arguments against this hypothesis). The structure of GCs is usually described with the parameters of the King (1966) model that best fits their Surface Brightness (SB) profile, that are the central SB $\mu(0)$, the *core radius* r_c and the concentration $C = \log(r_t/r_c)$, where r_t is the *tidal radius* (see King 1966, hereafter K66). Other fundamental parameters, not necessarily linked to K66 models, are the total absolute magnitude, usually reported in the V passband, M_V , and the half-light radius r_h .

Independently of the actual origin of NGC 2419, its peculiar structure is clearly an interesting subject of study. In this sense, it seems particularly important to check the reliability of the parameters that makes this clusters so special and worth of further investigations, that is its structural parameters and the SB profile they are obtained from. There are several independent estimates of (at least some) structural parameters of NGC 2419 (see, for example, Peterson & King (1975), Natali, Pedichini & Righini (1991), hereafter NPR, Cohen et al. (2006), and references therein), but the only publicly available SB profile is that provided by Trager, King & Djorgovski (1995, hereafter TKD) by assembling the observational material previously obtained with various methods and by various authors. The same observed profile was later re-analyzed by McLaughlin & van der Marel (2005, hereafter MvdM). While there is no particular reason to doubt of the reliability of the TKD profile, a check with a completely independent observed profile would be clearly valuable. I have obtained such a profile by combining three different datasets and two different techniques. This short note is aimed at reporting on this newly obtained profile and structural parameters and on the comparison with previously available data.

2. Data Analysis

The first dataset adopted for the analysis is a set of sky-subtracted drizzled images taken with the Advanced Camera for Surveys / Wide Field Channel (ACS/WFC) camera on board

of the Hubble Space Telescope (HST): a F475W image with $t_{exp} = 680$ s, a F606W image with $t_{exp} = 676$ s, a F814W image with $t_{exp} = 676$ s, and a F850LP image with $t_{exp} = 1020$ s¹, that were retrieved from the HST archive (images j8io01031_drz, j8io01081_drz, j8io01071_drz, and, j8io01041_drz, respectively, from the GO9666 program, P.I. L. Gilliland). The region within 21'' from the cluster center is fully enclosed in all these images. I obtained the SB profile in this region by aperture photometry on concentric, 3'' wide, annuli in all the four images². By definition, a surface density profile obtained with aperture photometry is completely unaffected by incompleteness, as opposite to profiles obtained from star counts. Therefore this portion of the profile will provide the fundamental benchmark to check the effects of radial variations of the completeness in the innermost part of the profile derived from star counts (see below). Moreover, the surface photometry can be reported to an absolute scale by means of the photometric Zero Points (ZP) of Sirianni et al. (2005). Normalizing the profile from star counts to the inner profile obtained from aperture photometry, the whole composite profile can be reported to the same absolute photometric scale.

I searched the center of symmetry of the cluster by computing the light density over apertures of radius = 4'' in many different positions around the apparent center of the cluster; the maximum was found at the image (pixel) coordinates $(x_0, y_0) = (610, 2895)$. Taking the astrometric solution embedded in the images as a reference, this is fully consistent with the position of the center that is available in the literature (Harris (1996)). Since the adopted center of the raster of annuli may be critical for the aperture photometry, I derived the profile by adopting seven different positions of the center of the annuli, i.e. $(x, y) = (x_0 \pm 10 \text{ px}, y_0)$, $(x, y) = (x_0, y_0 \pm 10 \text{ px})$, $(x, y) = (x_0 - 10 \text{ px}, y_0 + 10 \text{ px})$, $(x, y) = (x_0 + 10 \text{ px}, y_0 - 10 \text{ px})$, and, obviously $(x, y) = (x_0, y_0)$. The final SB value in each annulus is the average of the seven values obtained with the different assumptions on the coordinates of the center, and their standard deviation is the adopted uncertainty. The F606W and F814W profiles have been calibrated in the VEGAMAG system, while the F475W and F850LP profiles have been calibrated in the ABMAG system, using the ZPs by Sirianni (2005). The reason of the adoption of different systems will become clear below.

The aperture photometry profiles in the various passbands are compared in the upper panel of Fig. 1; arbitrary constants have been added to the F814W, F475W and F850LP profiles to match the Zero Point of the F606W profile. In this way the *shape* of the different profiles can be properly compared. The agreement among the different profiles is excellent. All previous determinations of the profile of NGC2419 were obtained from ground based data, in many cases with seeing width significantly larger than 1''. The profile for $r \leq 21''$ obtained here from ACS data is clearly superior to all of them and should be taken as the reference, in this range of distances from the cluster center. For each profile we measure the Half Width at Half Maximum (HWHM) length, that is a good initial proxy for r_c . From the average of the four values we obtain $\text{HWHM} = 18.0'' \pm 1.0''$.

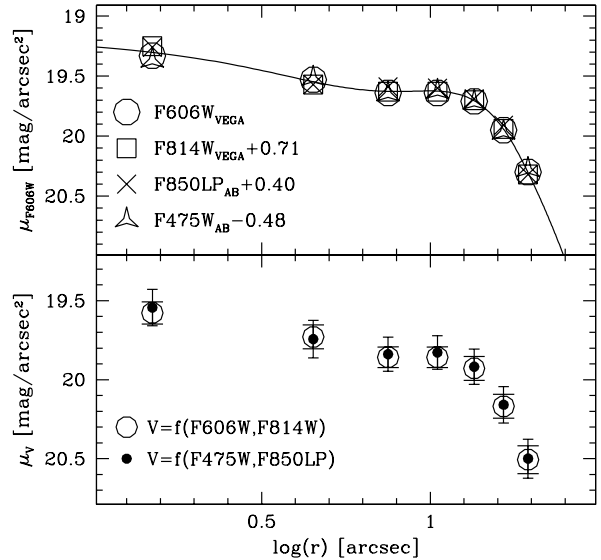


Fig. 1. Upper panel: observed Surface Brightness profile from aperture photometry within $r \leq 21''$ of the four ACS images considered here. An arbitrary normalization constant have been added to the F814W, F850LP and F475W profiles to match the zero point of the F606W profile. Note the virtually perfect match among the *shapes* of the various profiles. The continuous line is a cubic spline interpolated on the average of the four SB values. Lower panel: derived SB profiles in V obtained from (a) the F606W and F814W profiles (VEGAMAG system) and the transformation by G06 (large open circles), and (b) the F475W and F850LP profiles (ABMAG system) and the transformation by F07 (filled circles). The error bars include uncertainties in the zero points and in the transformations. Note the *excellent* match between the two *fully independent* profiles.

Galleti et al. (2006, hereafter G06) obtained a relation to transform F606W magnitudes into standard V magnitudes³, as a function of F606W-F814W color (VEGAMAG system). The V profile obtained by applying this relation to the observed F606W, F814W profiles is plotted in the lower panel of Fig. 1 (large empty circles). On the other hand, Federici et al. (2007, hereafter F07) obtained a relation to transform F475W magnitudes into standard V, as a function of F475W-F850LP color (ABMAG system). The V profile obtained by applying this relation to the observed F475W, F850LP profiles is also plotted in the same panel of Fig. 1 (filled circles). In both cases, uncertainties in the ZP and in the transforming relations have been included in the error bars. *The agreement between the two fully independent V profiles is excellent.* This further check, strongly support the reliability of the absolute surface photometry in the innermost 21'' of NGC 2419. In the following I will take the V profile obtained from the F606W, F814W profiles as the reference, since it is based on a less-scattered, more reliable photometric transformation (G06). From the derived V profile, $\mu_V(0) = 19.55 \pm 0.10$ is obtained, ~ 0.2 mag brighter than reported by TKD, but ~ 0.1 mag fainter than what found by MvdM from the same data as

¹ These are *total* exposure times of the *combined* drizzled images. The inspection of the images reveal that there is no heavily saturated star in the innermost 20'' region where aperture photometry has been performed.

² Using the XVISTA package, see <http://astronomy.nmsu.edu/holtz/xvista/index.html> and Lauer (1985).

³ In the Johnson-Kron-Cousins system, based on Landolt (1992) standard stars.

TKD. For the reasons outlined above, also the value of $\mu_V(0)$ obtained here should be regarded as very reliable.

Photometry of individual stars in the ACS images considered here were obtained by G06 and F07, to derive the relations between photometric systems. Here I use their F475W,F850LP Color Magnitude Diagram (CMD) to select the stars to count to extend the SB profile outside the small region covered by integrated aperture photometry. In the following we will refer to the adopted catalogue of positions and photometry of individual stars as to the ACS sample.

2.1. Ellipticity from integrated photometry

The ACS images are too small and off-centered to be used to obtain a global estimate of the ellipticity of the cluster. I have retrieved from the Italian Center of Astronomical Archives⁴ a $t_{exp}=240$ s V image of NGC2419 taken with the DOLORES camera⁵ at the Telescopio Nazionale Galileo (TNG), at the observatory Roque de Los Muchachos, in La Palma, Canary islands (Spain). The image was acquired in 2004, January 27, during a test session; the seeing was $\sim 1''$ FWHM. The pixel scale is $0.275''\text{px}^{-1}$. The image was corrected for bias and flat field with standard IRAF procedures and it was used to study the ellipticity of the cluster over the range $5'' \leq r \leq 120''$, i.e. approximately out to two times the half-light radius of the cluster (see below).

The ellipticity ($\epsilon = 1 - \frac{b}{a}$, where a and b are the semi-major and semi-minor axes, respectively) was computed by finding the ellipses that best fits the light distribution, while keeping fixed the center of the ellipses, using the XVIDA task *profile*, as described in detail in F07. This task computes the (elliptical) light profile adopting one pixel step: to reduce the noise I averaged all the derived quantities over $\pm 5''$ wide bins, as done in F07. The shape of the derived SB profile was in good agreement with the ACS profile, in the region of overlap.

The average ellipticity of NGC2419 over the considered radial range is $\epsilon = 0.19 \pm 0.15$, where the uncertainty is the standard deviation of the distribution. The average Position Angle, computed from North ($PA=0^\circ$) toward East ($PA=+90^\circ$), is $\langle PA \rangle = +105^\circ \pm 28^\circ$. The ellipticity and PA profiles are shown in Fig. 2. Except for a narrow peak in the range $10'' \lesssim r \lesssim 20''$, the ellipticity profile is always within $\pm 1\sigma$ from the overall mean. A 2σ clipping average excludes the four points of the profile with the highest ellipticity, leading to a slightly lower mean $\epsilon = 0.14 \pm 0.07$.

2.2. Star Counts

In Fig. 3 the photometric samples that have been used to derive the surface density profile from star counts on concentric annuli are presented. The innermost sample is constituted by the ACS/WFC photometry already described above (left panels). An intermediate sample is provided by the accurate photometry by Saha et al. (2005, hereafter S05; central panels); in particular this sample cover one full quadrant over a radial range that joins the ranges of the ACS sample and the outermost sample, that was retrieved from the Sloan Digital Sky Survey (Adelman-McCarthy et al. 2005, hereafter SDSS). Cluster stars are selected on the Color Magnitude Diagram (CMD) as shown in the lower panels of Fig. 3. The circles overplotted on the upper-panels maps of Fig. 3 shows that there are generous overlapping regions between the adopted samples.

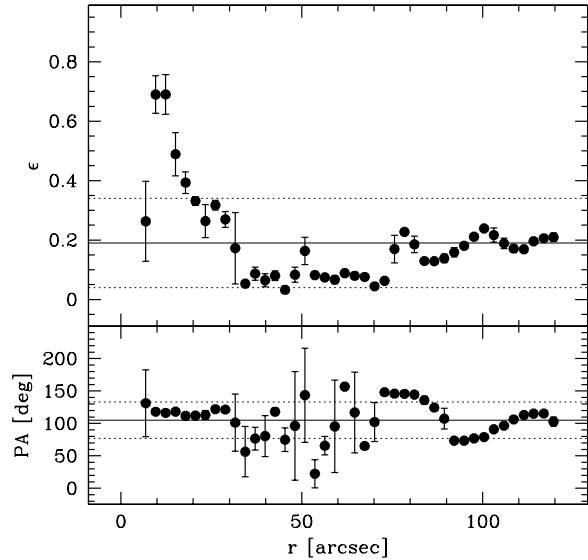


Fig. 2. Upper panel: ellipticity as a function of distance from the cluster center. The thin continuous line marks the value of the mean ellipticity, averaged over the whole radial range, the dotted lines are at $\pm 1\sigma$ from the mean. Lower panel: Position Angle as a function of distance from the cluster center. The lines have the same meaning as in the upper panel.

Surface density profiles were obtained from each sample, using different bin widths, according to the different density of tracer stars of the different samples and in each different radial range. Each sample is intended to cover a given radial range, and the corresponding profiles are compared (and matched) in the regions of overlap (see the circles superposed to the maps in the upper panels of Fig. 3), with a bootstrap process that uses as a reference the innermost profile from aperture photometry, and then, in turn, the ACS, the S05 and the SDSS samples. The effects of radial variations of the incompleteness can be checked by comparing with a profile that has been proven to be unaffected by this problem: if the profiles have the same shape in the region of overlap, the outer profile does not suffer from radially varying incompleteness (see Federici et al. 2007). For example, in the case of the ACS sample, surface density profiles were obtained from star counts by using different magnitude thresholds ($F850LP < 20$, $F850LP < 21$, ..., $F850LP < 23$) to select the tracer stars (brighter thresholds would correspond to more complete samples). The star count profile from the $F850LP < 20$ sample nicely matched the aperture photometry profile in the innermost $10''$, hence it is free from incompleteness problems in that range. The $F850LP < 22$ profile, that suffered from significant incompleteness for $r < 8''$, matched the $F850LP < 20$ profile for $r > 10''$, hence it was adopted in that range. Analogously, it was possible to adopt the $F850LP < 23$ for $r \geq 27''$, since there was excellent match with the $F850LP < 22$ profile for $r \gtrsim 20''$. In this way all the various profiles, from the various samples, were assembled into a single “star counts” profile that is unaffected by radial variations in the completeness.

The contribution of the background to the surface density was subtracted from whole profile obtained from star counts; the background density was estimated in the $720'' \leq r \leq 900''$ re-

⁴ IA2, at <http://www.oats.inaf.it/IA2/>

⁵ See <http://www.tng.iac.es/instruments/lrs/>

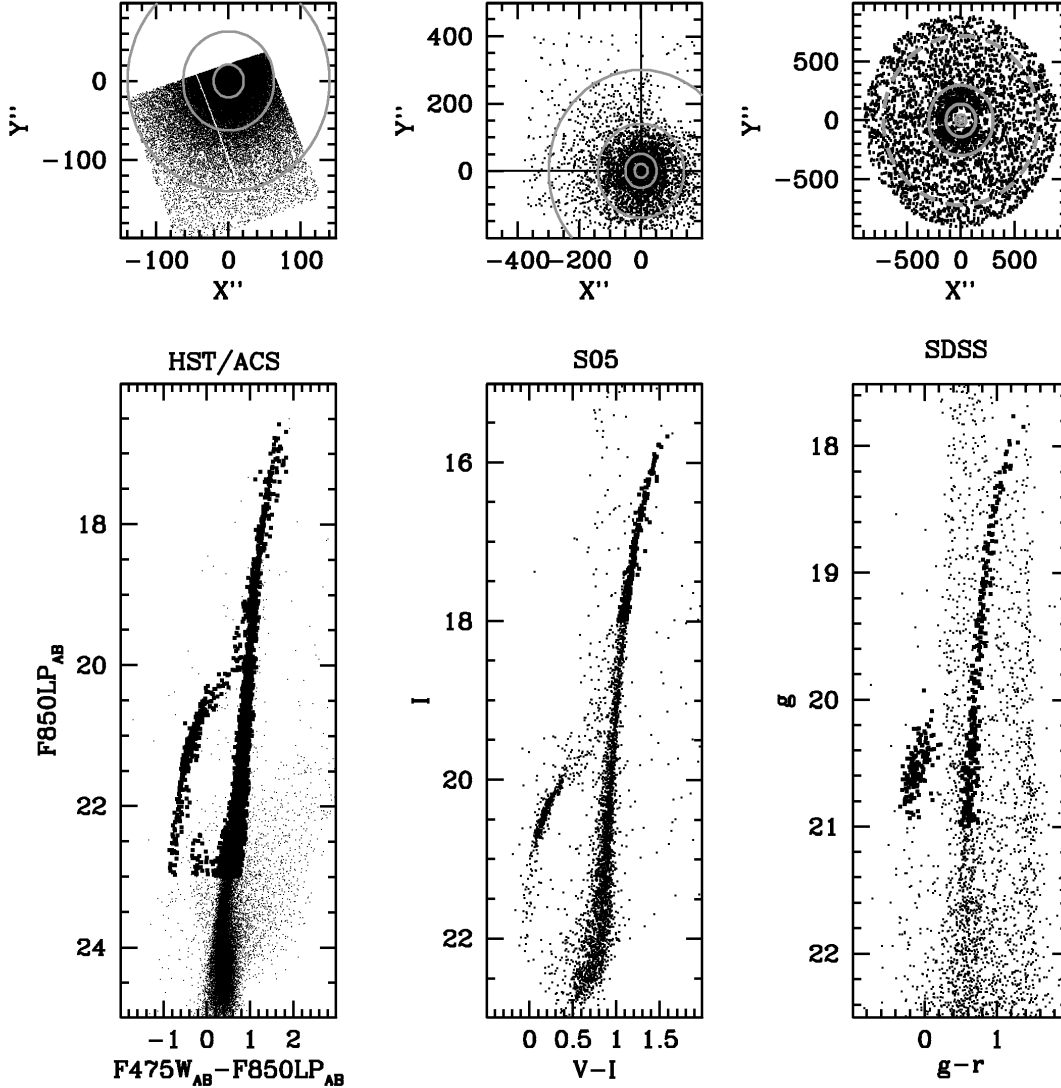


Fig. 3. Samples used for the star counts (upper panels: sky-projected maps; lower panels Color Magnitude Diagrams). The stars selected for the analysis are plotted as heavier dots in the CMDs. The grey circles plotted in the maps marks the boundaries between regions covered by a given dataset and/or the regions of overlap among the various datasets that have been used to derive the SB profile. In order of increasing radius: $r \leq 21''$: Aperture Photometry on ACS images; $21'' < r \leq 51''$: star counts on ACS data; $51'' < r \leq 140''$: region of overlap between the ACS and the S05 data (star counts); $140'' < r \leq 300''$: region of overlap between the S05 data (upper left quadrant) and the SDSS data (star counts); $r = 720'' = 12'$: (dashed circle) outer boundary for the star counts from the SDSS data. The background level was estimated in the area outside of this circle, up to $r = 15'$.

gion of the SDSS sample (see the upper right panel of Fig. 3), well beyond the tidal radius of the cluster ($r_t = 522''$, TKD). Finally the profile was matched to the V profile obtained from the aperture photometry to convert in calibrated SB units, and, finally, the combined profile reported in Tab. 1 was produced (Tab. 1 is available only in electronic form, in the on-line edition of this note). The profile from integrated photometry obtained from the TNG data (Sect. 2.1, above) was used to further check that the overall combined profile was well-behaved in the region where aperture photometry and star counts data have been joined.

The bright magnitude threshold adopted for the S05 and - to a lesser extent - for the SDSS sample (see Fig. 3) im-

plies that in the outer low-density regions of the cluster covered by these samples the uncertainty on the derived SB can be quite large, in some case. The accurate tracing of these parts of the profile would require much deeper wide-field photometry than what publicly available (see, for example, Ripepi et al. 2007). Moreover I excluded from the final profile all the annuli where the number of selected cluster stars were < 10 , hence the SB estimates of Tab. 1 are not necessarily regularly spaced. Nevertheless, (a) the reported SBs for $r \leq 51''$ are, by far, the most accurate estimates presently available, (b) the new profile covers a much larger radial range with respect to previously available ones (TKD), i.e. $r \approx 8' \approx 1r_t \approx 25r_c$, and, (c) it is obtained from datasets never used before for this purpose, thus

providing observational constraints on the structure of NGC2419 that are fully independent from what was already available in the literature.

3. Structural parameters for NGC 2419

In Fig. 4 we compare the profile of Tab. 1 with the theoretical profiles of isotropic single-mass K66 models, and with the combination of observed profiles adopted by TKD. In the upper panel, we adopt the central surface brightness and the HWHM values obtained in Sect. 2. The overall profile is best-fitted by a model with $C=1.35$, in good agreement with the results by TKD and MvdM. Adopting this model, the resulting core radius is $r_c = 1.07HWHM = 19.2''$, and the half-mass radius is $r_{hm} \approx 3.0r_c = 57.6''$. Since the relaxation time of NGC2419 is much larger than one Hubble time (Djorgovski (1993), MvdM), the effects of mass segregation should be very small in this cluster, hence the half-mass radius should be a good proxy for the half-light radius; for this reason I assume $r_h = r_{hm} = 57.6''$.

It is very interesting to note that *the newly (and independently) derived profile is in excellent agreement with the TKD profile for $r \geq 4''$* , with, perhaps, the exception of a small wiggle at $\log(r)=1.4$ in the region covered by ACS star counts. Given the initial purpose of the exercise reported in this note, i.e. to check the reliability of existing profiles, this result can be regarded as very reassuring. The only significant difference between the two profiles occurs at the innermost point: the TKD profile shows a curious drop in the inner few arcseconds. This lead TKD to derive a central SB much fainter than what found here, $\mu_V(0) = 19.77$ instead of $\mu_V(0) = 19.55$. Beyond the latest point of the TKD profile, for $r \gtrsim 290''$, the observed profile show a slight change of slope and a SB excess with respect to the best-fit King model. The feature is suggestive of the possible presence of extra-tidal stars (see Leon et al. (2000), F07, and also Ripepi et al. (2007)). However, given the typical uncertainties associated with this outer part of the profile, the feature is not further discussed in the following and it is not considered in the comparisons with TKD and with theoretical models.

The dashed line in the lower panel of Fig. 4 is a $C=1.40$ King's model with $\mu_V(0) = 19.77$: its comparison with the observed profiles shows that if such a faint central SB is adopted, a core radius as large as $r_c = 21''$ is needed to obtain a good fit at large radii. Therefore, the difference in the central SB is at the origin of the difference in the estimate of the core radius between the present analysis and TKD, that occurs in spite of the good agreement between the two profiles. On the other hand, if a core radius as large as $r_c = 21''$ and $\mu_V(0) = 19.55$ are simultaneously adopted, it is no more possible to obtain a good fit of the observed profile over the whole considered radial range ($r \leq 300''$) with a single King's model. A $C=1.1$ model is preferable for $r \lesssim 100''$, while a $C=1.3$ model is required at larger radii (Fig. 4, lower panel).

Since there is no reason to expect a central drop in the surface brightness, given the reliability of the aperture photometry profile derived here from ACS images, and since a unique fitting model for the whole radial range is preferable to two, I finally adopt the solution presented in the upper panel of Fig. 4, and the associated structural parameters, reported in the first column of Tab. 2.

To compute the total apparent integrated V magnitude I first derived the integrated magnitude within the central $20''$, through aperture photometry on the F606W image, finding $V_{r \leq 20''} = 12.27 \pm 0.05$, where the uncertainty is dominated by the uncertainties in the photometric zero points and in the transformations

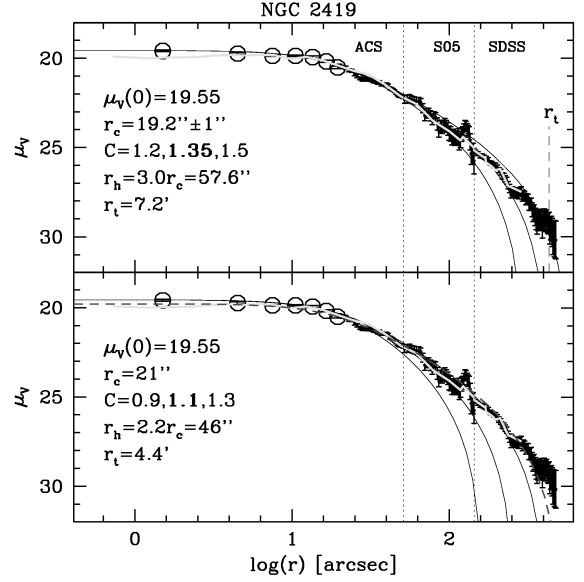


Fig. 4. Comparisons between the SB profile derived in the present analysis (open circles: from aperture photometry; small dots with errorbars: from star counts), the composite profile adopted by TKD (light grey line), and various King's models (thin continuous lines). Upper panel: adopting the new estimates of $\mu_V(0)$ and r_c , the observed profile is compared with King's models with $C=1.2, 1.35$, and 1.5 , from left to right. The best-fitting C value is written in boldface. The vertical dotted lines marks the boundaries between the portions of the profile obtained from different datasets. The dashed segment marks the position of the tidal radius of the best fit King model. Lower panel: the same as above but adopting the r_c value of TKD. In this case there is no model providing a good fit over the whole radial range and a C as low as 1.1 is required to fit the profile out to $r \sim 100''$. The grey dashed line is a $C=1.4$ king's model, adopting $\mu_V(0) = 19.77$, as done by TKD.

from F606W to V. Then I integrated the K66 model that best fits the observed profile ($C=1.35$) to estimate what fraction of the light is included in the innermost $20''$, $F_{20} = L_{r \leq 20''} / L_{r \leq r_t} = 0.191$. The total integrated magnitude is:

$$V_t = V_{r \leq 20''} + 2.5 \log(F_{20}) = 10.47 \pm 0.07 \quad (1)$$

Adopting $(m - M)_0 = 19.60 \pm 0.05$ and $E(B - V) = 0.08$, from Ripepi et al. (2007), the absolute integrated V magnitude is $M_V = -9.4 \pm 0.1$.

4. Summary

I have derived a new surface brightness profile for the remote globular cluster NGC2419 by using different datasets that were never used before for this purpose. This allowed me to verify the reliability and the accuracy of both *the shape and the photometric zero point* of previously existing profiles, as well as the accuracy of available estimates of the structural parameters for this peculiar and very interesting cluster. The main results of the present analysis can be summarized as follows:

- The agreement between the newly derived profile and the previously available one by TKD is more than satisfying.

Table 2. Structural Parameters of NGC 2419

Parameter	this work	TKD	MvdM	NPR	units
HWHM	18.0 ± 1.0	–	–	19.2	arcsec
r_c	0.32 ± 0.02	0.35	0.34	0.34	arcmin
C	1.35	1.4	1.38	1.5	–
r_h	0.96 ± 0.2	0.76	0.86	–	arcmin
r_t	7.1 ± 1.0	8.7	8.2	10.71 ^a	arcmin
$\mu_V(0)$	19.55 ± 0.10	19.77	19.44	–	mag/arcsec ²
V_t	10.47 ± 0.07	10.26 ^b	10.29	–	mag
M_V	-9.4 ± 0.1	-9.58	–	–	mag
$\langle \epsilon \rangle$	0.19 ± 0.15	–	–	–	–
$\langle \epsilon \rangle_{2\sigma}$	0.14 ± 0.07^c	–	–	–	–

^a From Peterson & King (1975).

^b From Peterson (1993).

^c Average obtained after the exclusion of the points of the ellipticity profile that deviated more than $2 - \sigma$ from the overall mean.

The overall agreement among the estimates of the main structural parameters from various sources is also sufficiently good (see Tab. 2). Therefore, it must be concluded that the structural parameters of NGC2419 are known with a good degree of reliability.

- The newly derived profile suggests a slight downward revision of the core radius, with respect to previous estimates, i.e. $r_c = 19.2'' \pm 1''$ instead of $r_c \gtrsim 20.5''$. The central SB derived here ($\mu_V(0) = 19.55$) is more similar to the estimate by MvdM ($\mu_V(0) = 19.44$) than to that by TKD ($\mu_V(0) = 19.77$). The less well constrained structural parameter is the tidal radius, that is extrapolated from the inner profile ($r \lesssim 290''$). The r_t value found here is slightly smaller with respect to previous analyses. This may have some effect on some related issues, as the possible detection of extra-tidal stars by Ripepi et al. (2007), and the estimate of the mass of the Milky Way obtained in Bellazzini (2004). The profile shows a slight break and a SB excess for $r \gtrsim 290''$ that may be indicative of the presence of an extra-tidal component (Leon et al. (2000)). The evidence is not conclusive and deserves to be followed-up with deeper wide-field photometry.
- The overall cluster shape is not so round, at least within $r \simeq 120''$, a radius enclosing significantly more than one half of the whole cluster light. The average ellipticity in this range is $\epsilon = 0.19 \pm 0.15$ (or $\epsilon = 0.14 \pm 0.07$, if a 2σ clipping algorithm is applied), a relatively high value for a globular cluster (see Barmby et al. 2007). Quite elongated shapes seem to be a typical characteristic of bright and large-sized clusters (see F07 and Galletti et al. 2007). The much lower values ($\epsilon = 0.03/0.04$, averaged over the whole cluster extent) found by Frank & Fall (1982) and White & Shawl (1987) may suggest a decrease of ellipticity at large radii.

Acknowledgements. The financial support to this research by the INAF-PRIN05 through the Grant CRA 1.06.08.02 is acknowledged. Based on observations made with the NASA/ESA Hubble Space Telescope, obtained from the Data Archive at the Space Telescope Science Institute, which is operated by the Association of Universities for Research in Astronomy, Inc., under NASA contract NAS 5-26555. These observations are associated with program GO9666. Based on observations made with the Italian Telescopio Nazionale Galileo (TNG) operated on the island of La Palma by the Fundación Galileo Galilei of the INAF (Istituto Nazionale di Astrofisica) at the Spanish Observatorio del Roque de los Muchachos of the Instituto de Astrofísica de Canarias. This research made use of data from the Sloan Digital Sky Survey. I'm grateful to Luciana Federici for an introduction to the basics of XVISTA. This research made use of the NASA/ADS database.

References

- Adelman-McCarthy, J.K., Agüeros, M.A., Allam, S.S., et al., 2006, ApJS, 162, 38 (SDSS)
- Barmby, P., McLaughlin, D., Harris, W.E., Harris, G.L.H., Forbes, D.A., 2007, AJ, 133, 2764
- Bellazzini, M., 2004, MNRAS, 347, 119
- Cohen J.G., Matthews K., Cameron P.B., 2006, ApJ, 634, L45
- Djorgovski, S.G., 1993, in Structure and Dynamics of Globular Clusters, S. Djorgovski and G. Meylan Eds., S. Francisco, ASP, ASP Conf. Ser., 50, 373
- Evstigneeva, E. A., Gregg, M. D., Drinkwater, M. J., Hilker, M., 2007, AJ, 133, 1722
- Federici, L., Bellazzini, M., Galletti, S., Fusi Pecci, F., Buzzoni, A., Parmeggiani, G., 2007, A&A, in press (arXiv:0706.2337)
- Frenk, C.S., & Fall, S.M., 1982, MNRAS, 199, 565
- Galletti, S., Federici, L., Bellazzini, M., Buzzoni, A., Fusi Pecci, F., 2006, ApJ, 650, L107 (G06)
- Galletti, S., Bellazzini, M., Federici, L., Buzzoni A., Fusi Pecci, F., 2007, A&A, in press, (arXiv:0705.4037)
- Harris, W.E. 1996, AJ, 112, 1487
- King, I.R., 1966, AJ, 71, 64 (K66)
- Landolt, A.U., 1992, AJ, 104, 340
- Lauer, T.R., 1985, ApJS, 57, 473
- Leon, S., Meylan G., Combes, F., 2000, A&A, 2000, 359, 907
- McLaughlin, D.E., van der Marel R.P., 2005, ApJS, 161, 304 (MvdM)
- Mackey, A.D., van den Bergh, S., 2005, MNRAS, 360, 631
- Natali, G., Pedichini, F., Righini, M., 1991, A&A, 248, 426 (NPR)
- Olszewski, E.W., Pryor, C., Schommer, R.A., in The Globular Cluster - Galaxy Connection, G.H. Smith and J.P. Brodie Eds., S. Francisco, ASP, ASP Conf. Ser., 48, 99
- Peterson, J., King, I.R., 1975, 1975, AJ, 80, 427
- Peterson, C.J., 1993, in Structure and Dynamics of Globular Clusters, S. Djorgovski and G. Meylan Eds., S. Francisco, ASP, ASP Conf. Ser., 50, 337
- Ripepi, V., Clementini, G., Di Criscienzo, M., et al., 2007, ApJ Letters, in press
- Saha, A., Dolphin, A. E., Thim, F., Whitmore, B., 2005, PASP, 117, 37 (S05)
- Sirianni, M., et al., 2005, PASP, 112, 925
- Trager, S.C., King, I.R., Djorgovski, S., 1995, AJ, 109, 218 (TKD)
- van den Bergh, S., 1995, AJ, 108, 2145
- White, R.E., & Shawl, S.J., 1987, ApJ, 317, 246

Online Material

Table 1. Observed surface brightness profile of NGC 2419

r arcsec	μ_V mag/arcsec ²	err_{μ_V} mag/arcsec ²	Technique ^a	Dataset
1.5	19.58	0.05	AP	ACS
4.5	19.73	0.06	AP	ACS
7.5	19.86	0.04	AP	ACS
10.5	19.86	0.04	AP	ACS
13.5	19.93	0.06	AP	ACS
16.5	20.17	0.06	AP	ACS
19.5	20.51	0.07	AP	ACS
20.0	20.42	0.09	SC	ACS
21.0	20.48	0.09	SC	ACS
22.0	20.53	0.09	SC	ACS
23.0	20.67	0.09	SC	ACS
24.0	20.70	0.09	SC	ACS
25.0	20.88	0.10	SC	ACS
26.0	20.99	0.10	SC	ACS
27.0	21.13	0.08	SC	ACS
28.0	21.20	0.08	SC	ACS
29.0	21.15	0.08	SC	ACS
30.0	21.21	0.08	SC	ACS
31.0	21.19	0.07	SC	ACS
32.0	21.24	0.07	SC	ACS
33.0	21.30	0.08	SC	ACS
34.0	21.32	0.07	SC	ACS
35.0	21.38	0.08	SC	ACS
36.0	21.32	0.07	SC	ACS
37.0	21.47	0.08	SC	ACS
38.0	21.47	0.08	SC	ACS
39.0	21.47	0.08	SC	ACS
40.0	21.45	0.07	SC	ACS
41.0	21.52	0.08	SC	ACS
42.0	21.68	0.08	SC	ACS
43.0	21.73	0.08	SC	ACS
44.0	21.78	0.08	SC	ACS
45.0	21.85	0.08	SC	ACS
46.0	21.95	0.08	SC	ACS
47.0	22.03	0.09	SC	ACS
48.0	22.10	0.09	SC	ACS
49.0	22.11	0.09	SC	ACS
50.0	22.13	0.09	SC	ACS
51.0	22.17	0.09	SC	ACS
52.0	22.30	0.22	SC	S05
54.0	22.29	0.22	SC	S05
56.0	22.25	0.21	SC	S05
58.0	22.33	0.21	SC	S05
60.0	22.37	0.21	SC	S05
62.0	22.40	0.21	SC	S05
64.0	22.40	0.21	SC	S05
66.0	22.47	0.22	SC	S05
68.0	22.80	0.25	SC	S05
70.0	23.21	0.29	SC	S05
72.0	23.09	0.27	SC	S05
74.0	23.06	0.26	SC	S05
76.0	23.23	0.29	SC	S05
78.0	23.42	0.31	SC	S05
80.0	23.28	0.29	SC	S05
82.0	23.31	0.28	SC	S05
84.0	23.68	0.34	SC	S05
86.0	24.05	0.38	SC	S05
88.0	23.84	0.34	SC	S05
90.0	23.87	0.35	SC	S05
92.0	23.78	0.32	SC	S05
94.0	23.70	0.33	SC	S05
96.0	23.81	0.33	SC	S05
98.0	23.96	0.35	SC	S05
100.0	24.20	0.40	SC	S05
102.0	24.24	0.41	SC	S05
104.0	24.42	0.44	SC	S05
106.0	24.42	0.44	SC	S05
108.0	24.47	0.41	SC	S05
110.0	24.47	0.41	SC	S05
112.0	24.47	0.41	SC	S05
114.0	24.37	0.42	SC	S05
116.0	24.69	0.45	SC	S05
118.0	24.57	0.45	SC	S05
120.0	24.28	0.39	SC	S05
122.0	24.20	0.36	SC	S05
124.0	24.02	0.34	SC	S05
126.0	23.78	0.30	SC	S05
128.0	23.81	0.28	SC	S05
130.0	23.99	0.33	SC	S05
132.0	24.09	0.33	SC	S05
134.0	24.20	0.36	SC	S05
136.0	24.69	0.45	SC	S05

Table 1. continued

r	μ_V	err_{μ_V}	Technique	Dataset
arcsec	mag/arcsec ²	mag/arcsec ²	^a	
138.0	25.35	0.60	SC	S05
140.0	25.35	0.60	SC	S05
142.0	25.35	0.60	SC	S05
144.0	25.76	0.72	SC	S05
147.5	25.25	0.11	SC	SDSS
152.5	25.35	0.11	SC	SDSS
157.5	25.46	0.12	SC	SDSS
162.5	25.49	0.12	SC	SDSS
167.5	25.55	0.12	SC	SDSS
172.5	25.61	0.12	SC	SDSS
177.5	25.69	0.12	SC	SDSS
182.5	25.87	0.13	SC	SDSS
187.5	25.91	0.13	SC	SDSS
192.5	25.99	0.14	SC	SDSS
197.5	26.02	0.14	SC	SDSS
202.5	26.13	0.14	SC	SDSS
207.5	26.27	0.15	SC	SDSS
212.5	26.38	0.16	SC	SDSS
217.5	26.59	0.17	SC	SDSS
222.5	26.62	0.17	SC	SDSS
227.5	26.75	0.18	SC	SDSS
232.5	26.86	0.19	SC	SDSS
237.5	27.12	0.21	SC	SDSS
242.5	27.30	0.23	SC	SDSS
247.5	27.57	0.27	SC	SDSS
252.5	27.45	0.25	SC	SDSS
257.5	27.57	0.26	SC	SDSS
262.5	27.49	0.25	SC	SDSS
267.5	27.57	0.25	SC	SDSS
272.5	27.59	0.26	SC	SDSS
277.5	27.62	0.26	SC	SDSS
282.5	27.50	0.24	SC	SDSS
287.5	27.43	0.23	SC	SDSS
292.5	27.74	0.27	SC	SDSS
297.5	27.66	0.25	SC	SDSS
302.5	27.73	0.26	SC	SDSS
307.5	27.92	0.29	SC	SDSS
312.5	27.88	0.28	SC	SDSS
317.5	27.90	0.28	SC	SDSS
322.5	28.18	0.33	SC	SDSS
327.5	28.20	0.33	SC	SDSS
332.5	28.15	0.32	SC	SDSS
337.5	28.50	0.39	SC	SDSS
342.5	28.72	0.44	SC	SDSS
347.5	28.64	0.42	SC	SDSS
352.5	28.89	0.49	SC	SDSS
357.5	29.06	0.54	SC	SDSS
362.5	29.24	0.61	SC	SDSS
367.5	29.11	0.55	SC	SDSS
372.5	29.00	0.51	SC	SDSS
377.5	29.02	0.51	SC	SDSS
382.5	28.92	0.47	SC	SDSS
387.5	29.07	0.52	SC	SDSS
392.5	29.42	0.66	SC	SDSS
397.5	29.12	0.53	SC	SDSS
402.5	28.89	0.46	SC	SDSS
407.5	29.17	0.54	SC	SDSS
412.5	29.06	0.50	SC	SDSS
417.5	28.96	0.47	SC	SDSS
422.5	29.24	0.56	SC	SDSS
427.5	29.27	0.57	SC	SDSS
432.5	29.15	0.52	SC	SDSS
437.5	29.67	0.75	SC	SDSS
442.5	29.51	0.66	SC	SDSS
447.5	29.53	0.67	SC	SDSS
452.5	29.76	0.79	SC	SDSS
457.5	30.04	0.97	SC	SDSS
467.5	30.11	1.02	SC	SDSS
472.5	30.15	1.04	SC	SDSS
477.5	30.18	1.06	SC	SDSS

^a AP = Aperture Photometry; SC= Star Counts.